Arabian Journal of Chemistry (2019) **12**, 236–248

King Saud University

Arabian Journal of Chemistry

www.ksu.edu.sa
www.sciencedirect.com

ORIGINAL ARTICLE

The effect of Variamine Blue B on brass corrosion in NaCl solution

Hülya Keleş *, **Süleyman Akça**

Osmaniye Korkut Ata University, Faculty of Arts and Science, Department of Chemistry, 80000 Osmaniye, Turkey

Received 4 November 2014; accepted 11 February 2015
Available online 25 February 2015

KEYWORDS

Brass;
Corrosion;
Electrochemical impedance spectroscopy;
ATR-FTIR;
NaCl;
Variamine Blue B

Abstract The effect of Variamine Blue B (4-Amino-4′-Methoxydiphenylamine-Diazonium Chloride, VBB) on the corrosion of Cu–35Zn alloy (brass) in 3.5% NaCl medium was studied at different concentrations and temperatures. For this purpose, electrochemical impedance spectroscopy (EIS) and potentiodynamic polarization techniques were used as electrochemical techniques. Scanning electron microscopy (SEM) and attenuated total reflectance Fourier transform infrared spectroscopy (ATR-FTIR) was used as optical techniques to investigate the brass surface. According to experimental results, inhibitor effectiveness increased with increasing temperature and VBB reduced the corrosion rate by acting as a mixed type inhibitor. The activation energy (E_a) of the dissolution process and the standard free energy values ΔG^{o}_{ads} of the adsorption process showed that chemical interactions also had a minor contribution to the adsorption of VBB on brass surface while physical interactions had a major one. Electrochemical and optical results revealed that VBB molecules held persistently on brass surface even after 120 h. The existence of VBB on brass surface was verified experimentally by ex-situ ATR-FTIR spectroelectrochemical measurement.

1. Introduction

Brass is an alloy (Cu–Zn) which is commonly used in extensive industrial applications and for esthetic purposes (Fan et al., 2011). Brass finds a wide range of applications in industrial processes because of its electrical and thermal conductivity facilities. Also good machinability, corrosion resistance, and low cost are features which make brass suitable for marine environments, heat exchanger tubes and absorption refrigeration systems (Xavier et al., 2012). Despite the high corrosion resistance of copper and its alloys in atmospheric conditions these metals may easily give dissolution reactions in marine environments. Especially chloride and bromide ions promote the dissolution of copper and its alloys (Ma et al., 2002).

Copper and its alloys undergo electrodissolution in marine environments and there are numerous investigations related with the inhibition of the corrosion of these metals with organic compounds (Gerengi and Bereket, 2012). Recently nitrogen containing heterocyclic compounds have attracted great interest being used as inhibitors against corrosion of copper and its

* Corresponding author. Tel.: +90 328 827 10 00/2538; fax: +90 328 827 1030.
E-mail address: hulyakeles@osmaniye.edu.tr (H. Keleş).
Peer review under responsibility of King Saud University.

ELSEVIER Production and hosting by Elsevier

http://dx.doi.org/10.1016/j.arabjc.2015.02.007
1878-5352

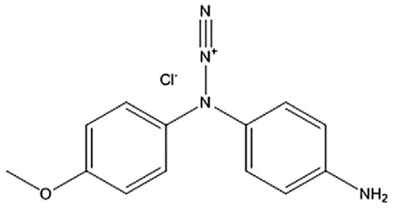

Figure 1 Variamine Blue B salt (4-Amino-4′-Methoxydiphenylamine-Diazonium Chloride, $C_{13}H_{12}ClN_3O$).

alloys. It has been repeatedly reported (Solmaz et al., 2011) that compounds containing nitrogen and/or sulfur atoms can co-ordinate with metals to form chelates. Benzotriazole (BTA) is the one of the best known corrosion inhibitors (Ravichandran and Rajendran, 2005) and many researchers have investigated the inhibitory effect of BTA in chloride environment (Gerengi et al., 2009, 2010; Kosec et al., 2007, 2008; Antonijevic et al., 2005, 2009). Mountassir and Srhiri (2007) have investigated the inhibitory effect of aminotriazole on the corrosion and dezincification of Cu–40Zn in chloride solution including sulfide ions as accelerators and concluded that the aminotriazole is an effective inhibitor. Özkir et al. (2013) have reported that the addition of hyamine in HNO_3 medium inhibited the corrosion of brass.

The present work focuses on the behavior of Variamine Blue B as an inhibitor for corrosion of Cu–35Zn brass in 3.5% NaCl solution at different temperatures. The electrochemical behaviors of brass were studied using potentiodynamic polarization technique (Tafel curves) and electrochemical impedance spectroscopy (EIS) in the absence and presence of Variamine Blue B. The morphologies of the brass surface examined with SEM technique and ATR-FTIR technique were used for verifying existence of VBB on the samples after 120 h exposing with corrosive medium.

2. Material and methods

2.1. Sample preparation

A brass specimen with the composition Cu: 59.2945; Zn: 35.7533; Pb: 2.6114; Sn: 1.7891; Ni: 0.2776; Fe: 0.2742 was used. The chemical composition analyze was done with a PAN Analytical brand AXIOS Advanced model XRF equipment. In order to expose the corrosive environment, the specimen was embedded in epoxy resin except the circular bottom whose area was 0.773 cm^2. Before the measurements, the brass surface was mechanically abraded using emery papers with different grades the highest being 1200. Respectively, the electrode surface was degreased and cleaned by rinsing with acetone and distilled water.

2.2. Testing environment

The chemicals NaCl (Merck) and VBB (Sigma–Aldrich) were used as purchased. The test solutions were prepared as % mass in volume (w/v) using 3.5% NaCl solution without and with the addition of different concentrations of VBB. The concentrations ranged from 1.0×10^{-4} mol/L to 1.25×10^{-3} mol/L. The molecular formula of VBB (4-Amino-4′-Methoxydiphenylamine-Diazonium Chloride) is given in Fig. 1.

2.3. Electrochemical measurements

Electrochemical measurements were carried out using a CHI 608d model electrochemical analyzer controlled with a computer. The standard three-electrode cell configuration was used for electrochemical measurements. A brass electrode with a known composition was used as the working electrode, a platinum sheet as the auxiliary (2 cm^2) and an Ag/AgCl electrode as the reference electrode. During the measurements solutions were kept open to the atmosphere and the temperatures were controlled with a thermostat range 298–328 K. All measurements were done after an immersion time of 1 h without stirring the test solutions and were repeated at least three times until the same result was obtained.

The potentiodynamic curves were obtained in two parts: The first was from E_{corr} to −0.60 V as a cathodic side with a scan rate of 0.001 Vs^{-1}. After cleaning the surface the anodic side was obtained from E_{corr} to 0.24 V with the same scan rate. The corrosion rates were calculated by extrapolation of linear region of the cathodic plots.

EIS measurements were taken at a steady-state open circuit potential (E_{ocp}), sine wave voltage with perturbation amplitude of 0.005 V peak to peak, at frequencies between 100 kHz and 10 mHz. The impedance diagrams were given using the Nyquist representation and multiplied with the surface area (0.773 cm^2). Zview software program (Scribner Associates Inc.) was used for analysing impedance values.

2.4. Surface investigations

The surface visualization of the brass samples was carried out after 120 h immersion time in corrosive media, by a ZEISS/EVO LS10 (Serial number: 354700 9924/2476) scanning electron microscope.

Attenuated total reflectance Fourier transform infrared spectroscopy (ATR-FTIR) was used for brass surface investigations before and after immersion in 3.5% NaCl solution absence and presence of 1.25×10^{-3} mmol/L VBB. The ATR-FTIR spectra measurements were performed by using a Perkin Elmer Spectrum 65 model Spectrophotometer. (Serial number: 87503).

3. Results and discussion

3.1. Potentiodynamic polarization studies

The representative potentiodynamic polarization curves of brass in 3.5% NaCl solution in the absence and presence of various concentrations of VBB after mentioned immersion time are shown in Figs. 2 and 3. The corrosion current density (i_{corr}) values were determined by extrapolation of Tafel lines to the corresponding corrosion potentials. All calculated i_{corr} values in the absence and presence of different concentrations of VBB are given in Table 1. The table represents the corrosion potential (E_{corr}), corrosion current density (i_{corr}), corrosion rate (C_R) in terms of (mm/year) and inhibition efficiency

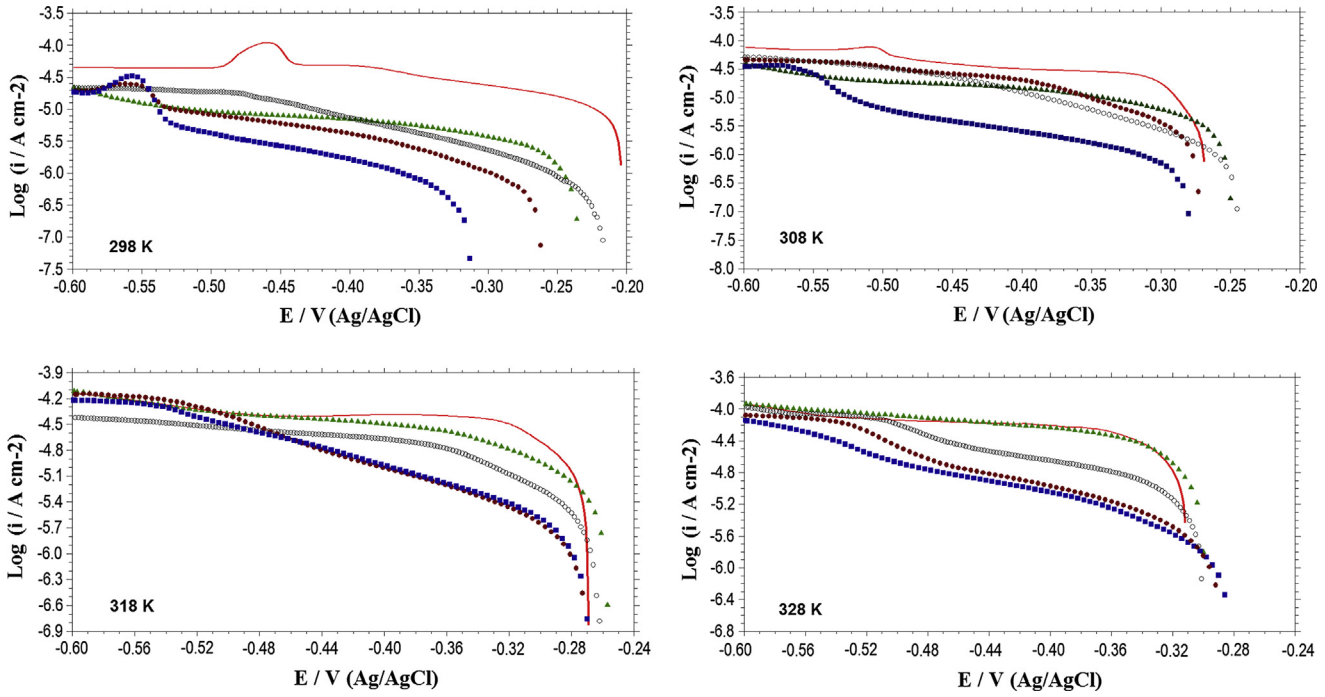

Figure 2 Cathodic polarization curves of brass in 3.5% NaCl at different VBB concentrations and temperatures. (——) none, (▲) 0.1, (○) 0.5, (●) 1.0, and (■) 1.25 mmol/L VBB.

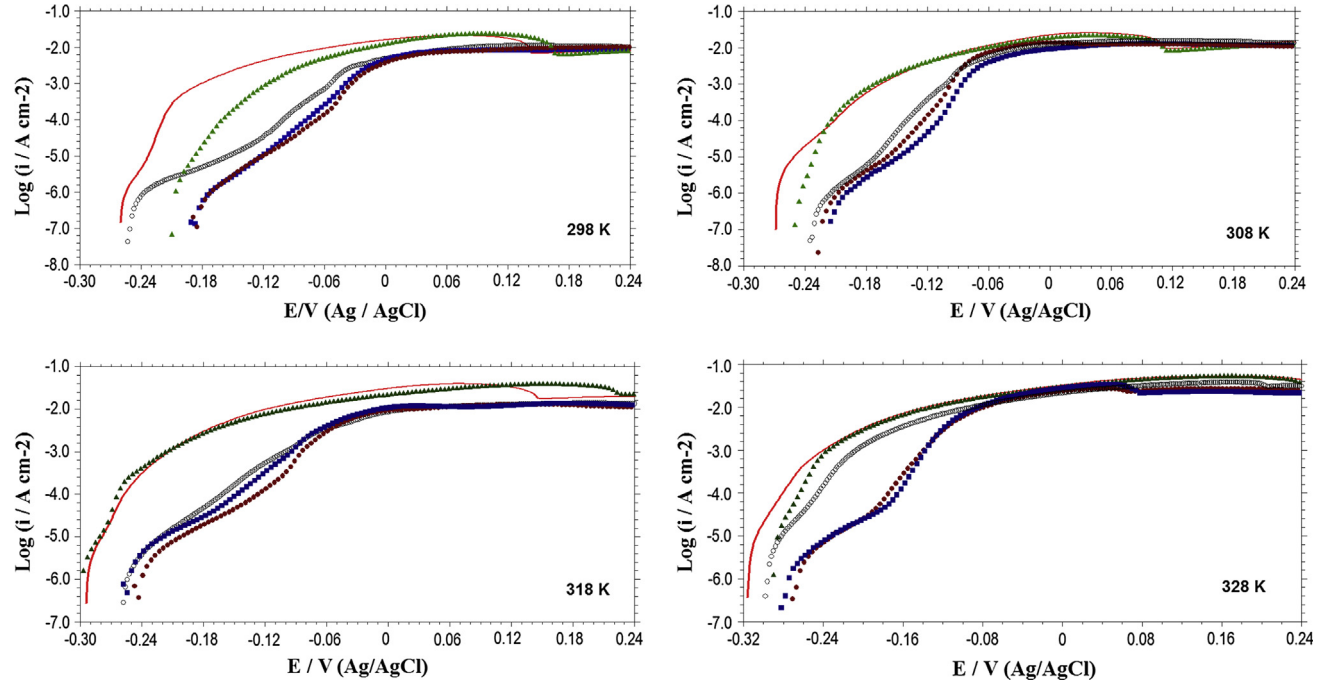

Figure 3 Anodic polarization curves of brass in 3.5% NaCl at different VBB concentrations and temperatures. (——) none, (▲) 0.1, (○) 0.5, (●) 1.0 and, (■) 1.25 mmol/L VBB.

percent (*IE*%). The corrosion rates were calculated as described previously (Keleş, 2011).

The inhibition efficiency was calculated from the polarization data as in Eq. (1)

$$IE\% = \frac{i_{corr} - i'_{corr}}{i_{corr}} \times 100 \quad (1)$$

where i'_{corr} and i_{corr} are the corrosion current densities in solutions with and without an inhibitor, respectively.

3.1.1. Cathodic curves

The cathodic polarization curves of the Cu–35Zn alloy in 3.5% NaCl solution with different concentrations of VBB at different temperatures are represented in Fig. 2.

Table 1 Tafel polarization parameters for the corrosion of brass in 3.5% NaCl solution containing different concentrations of VBB at various temperatures.

T (K)	C (mmol/L)	E_{corr} (V)	i_{corr} (μA cm^{-2})	Corrosion rate (mm/year)	Inhibition efficiency IE%
298	–	−0.204	11.966	0.138747	–
	0.1	−0.236	2.438	0.028269	79.6
	0.5	−0.217	0.7071	0.008199	94.1
	1.0	−0.262	0.6323	0.007332	94.7
	1.25	−0.313	0.6131	0.007109	94.9
308	–	−0.269	23.903	0.277158	–
	0.1	−0.250	4.220	0.048931	82.3
	0.5	−0.273	2.425	0.028118	89.9
	1.0	−0.245	1.199	0.013903	95.0
	1.25	−0.280	0.764	0.008859	96.8
318	–	−0.269	32.031	0.371403	–
	0.1	−0.257	6.851	0.079438	78.6
	0.5	−0.262	2.849	0.033034	91.1
	1.0	−0.269	1.889	0.021892	94.1
	1.25	−0.270	1.018	0.011804	96.8
328	–	−0.312	52.82	0.612453	–
	0.1	−0.300	37.94	0.439918	28.2
	0.5	−0.301	10.73	0.124415	79.7
	1.0	−0.288	2.94	0.034090	94.4
	1.25	−0.282	2.17	0.025161	95.9

The figure reveals that adding VBB increasingly in the corrosive solution decreased the cathodic current densities, and because no significant change was detected in the appearance of the cathodic curves it can be said that the cathodic process was unchanged. This indicates the adsorption of VBB molecules on the brass surface and the retardation of corrosion without altering the cathodic reaction mechanism by merely blocking the active sites (Oguzie et al., 2007). In the cathodic range, dissolved oxygen in the solution takes over the cathodic reaction of brass in 3.5% NaCl media as shown in the following Eq. (2)

$$O_2 + 2H_2O + 4e^- \rightarrow 4OH^- \quad (2)$$

It is clear from Table 1 that i_{corr} values decreased and IE% increased when the VBB concentration was increased, indicating an inhibiting effect. The currents of potentials more negative than −0.55 V disclose the mass transport in the cathodic process, for the temperatures 298 K and 308 K. Mountassir and Srhiri (2007) point out that the reduction of oxygen reaction is a mixed type of process including diffusion and activation processes. It was observed that in the activation controlled region (Tafel) currents were almost linear. After the mentioned potential the currents do not increase linearly due to the diffusion controlled reaction. A similar situation was observed at 318 K and 328 K temperatures. This behavior could be explained in the following manner: the oxygen diffusion decreased in high temperatures due to the decrease of oxygen solubility in water. Therewith the concentration of O_2 molecules which reached the metal surface was limited and the currents did not increase even at more negative potentials than −0.50 V. Similar results have been also reported in literature on the suppression of cathodic reaction of metals (Qi et al., 2013; Kear et al., 2005).

3.1.2. Anodic curves

The anodic curves obtained in 3.5% NaCl solution VBB free and with different concentrations of VBB are shown in Fig. 3.

Fig. 3 reveals that, the addition of VBB caused a decrease in anodic current densities and presents the modification on the shape of the anodic curve. The accepted explanation of anodic dissolution mechanism of brass in neutral chloride media can be outlined as follows: In the beginning of the corrosion stage, the ZnO layer is formed on brass surface via the reaction,

$$Zn^{2+} + H_2O \rightarrow ZnO + 2H^+ \quad \text{or} \quad (3)$$

$$Zn + H_2O \rightarrow ZnO + 2H^+ + 2e^- \quad (4)$$

Also at this time copper forms Cu_2O according to the following reaction, (Ravichandran et al. 2004; Gao and Liang, 2007).

$$2Cu^+ + H_2O \rightarrow Cu_2O + 2H^+ \quad \text{or} \quad (5)$$

$$2Cu + H_2O \rightarrow Cu_2O + 2H^+ + 2e^- \quad (6)$$

These oxide layers occur immediately after the initial contact of brass with the chloride solution and they cannot prevent further anodic polarization of the metal. Chloride ions facilitate the dissolution of brass at more anodic potentials by formation of CuCl and $CuCl_2^-$ species as given in reactions (7)–(9). It is reported in literature that at this stage the anodic current is related with both charge and mass transfer processes (Ravichandran et al., 2004; Kear et al., 2005).

$$Cu^+ + Cl^- \rightarrow CuCl \quad (7)$$

The formed CuCl may also go through a disproportionation reaction resulting soluble species as follows (Ravichandran et al., 2004):

$$2CuCl \rightarrow Cu + CuCl_2 \quad (8)$$

$$CuCl + Cl^- \rightarrow CuCl_2^- \quad (9)$$

Addition of the inhibitor also mostly caused the E_{corr} shift toward more positive potentials than blank solution with

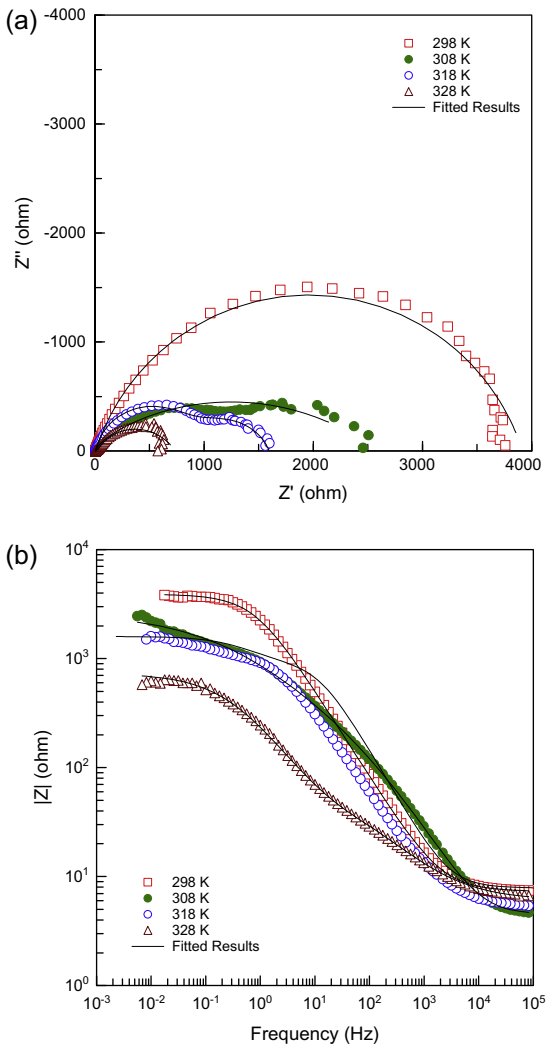

Figure 4 Nyquist diagrams (a) and Bode plots (b) of brass in 3.5% NaCl solution at different temperatures.

increased concentrations of VBB and at all temperatures. It is clear that the addition of VBB in a blank solution did not affect the dissolution mechanism of brass. A little plateau was observed at the anodic potentials which indicates the adsorption of VBB to form a protective film on the brass surface. As a consequence, the dissolution rate of brass decreased and the anodic reaction was controlled. The decrease in corrosion current densities was observed at high inhibitor concentrations even at the highest studied temperature. In literature, this observation is attributed to copper (I) complex formation with inhibitor molecule (Ma et al., 2002; Solmaz et al., 2011). However the inhibitor could not prevent the dissolution of metal after certain potentials at any of the studied temperatures. At this moment the desorption rate of the inhibitor molecules was greater than the adsorption rate which led to an increase in current densities to a certain value. The corrosion of brass occurred at open points of metal surface because an insufficient number of molecules could not cover these active sites at low concentrated VBB solutions.

$$CuCl_2^- \leftrightarrow Cu^{2+} + 2Cl^- + e^- \quad (10)$$

The Eq. (10) explains what happened at higher anodic over voltage. The current density increased because under high potentials Cu (II) species is formed from Cu (I). Even at higher potentials, the current density is controlled by diffusion limitations.

It can be concluded from potentiodynamic polarization curves that, there is a decrease in both cathodic and anodic current densities with the increase in VBB concentration at all temperatures. This confirmed that the addition of VBB has retarded the rates of both cathodic and anodic; namely oxygen reduction and metal dissolution reactions.

3.2. Electrochemical impedance spectroscopy (EIS) studies

The corrosion behavior of the Cu–35Zn alloy was investigated in 3.5% NaCl solution, in the absence Fig. 4 and presence of different concentrations of VBB Fig. 5 by using EIS technique at temperature range of 298–328 K. Nyquist and Bode plots of mentioned experimental conditions were presented, respectively.

In Figs. 4 and 5, it is seen that the impedance diagrams resemble a depressed semicircle, which is considered as typical behavior for solid electrodes observed in scattered impedance data (Gao and Liang, 2007). There are several reasons for this: Surface roughness, impurities, dislocations, grain boundaries, adsorption of inhibitors, etc. may cause this depressed view of Nyquist diagrams. The term 'disturbed capacitance' is used to characterize these types of Nyquist diagrams and, a constant phase element *CPE* is used instead of double layer capacity (C_{dl}) to explain the non-ideal behavior of the metal solution interface (Özcan, 2008). Related impedance of *CPE* is calculated according to Eq. (11) (Ahamad et al., 2010):

$$Z_{CPE} = \frac{1}{Y_o(j.w)^n} \quad (11)$$

where Y_o is the *CPE* constant, n is the *CPE* exponent. j is the square root of -1, and w is the angular frequency. Depending on the value of n, *CPE* can represent a resistance. n is a measure of non-ideality of the capacitor and has a value ranging from -1 to 1 (Negm et al., 2011).

EIS measurements demonstrated that the impedance response of brass changed in the presence of VBB in 3.5% NaCl solution. The change was significantly related to the adsorption of VBB molecules at the metal/solution interface. The diameters of capacitive loops were increased with the increasing of the concentration of VBB which indicates an increase in the polarization resistance of brass corrosion. The increase in resistance of Nyquist diagrams proved an increase in surface coverage. This can be seen distinctly from Fig. 5. The adsorbed inhibitor molecules form a protective film via insulating (Fengling et al., 2008) the brass surface from solution and making the corrosion reaction more difficult.

The physical description of the corrosion process of brass in the studied medium was analyzed by modeling the metal/solution interface to an equivalent electrical circuit. The EIS data were fitted to the most probable equivalent circuit for modeling metal/solution interface; therefore two types of equivalent circuits were proposed (Fig. 6).

In Fig. 6a an equivalent circuit with one semicircle was used for describing the inhibitor free brass/solution interface at 298 K. The elements of the circuit can be named as; R_s is the

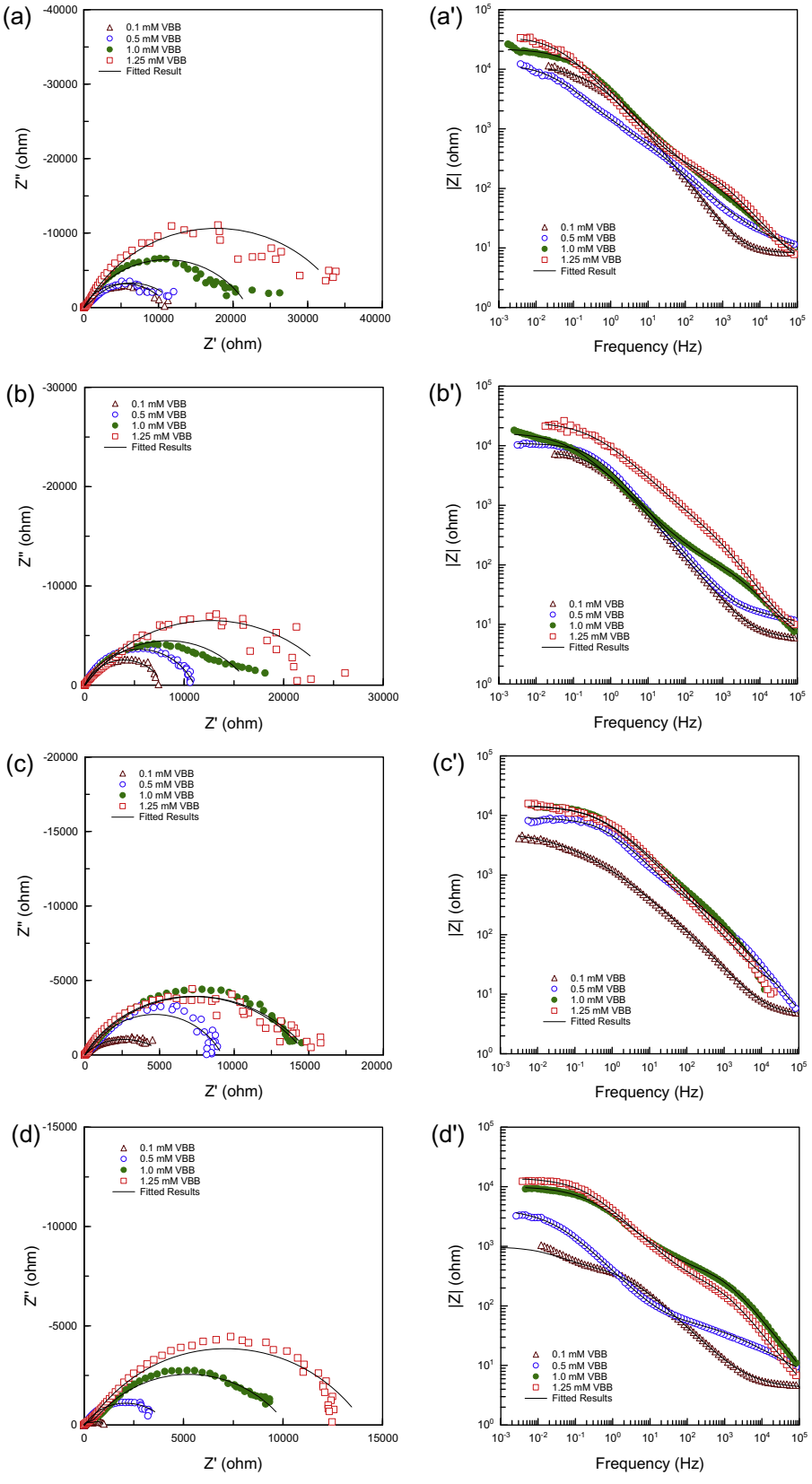

Figure 5 Nyquist and Bode plots of brass in 3.5% NaCl at different concentrations of VBB at (a and a′) 298 K, (b and b′) 308 K, (c and c′) 318 K and (d and d′) 328 K.

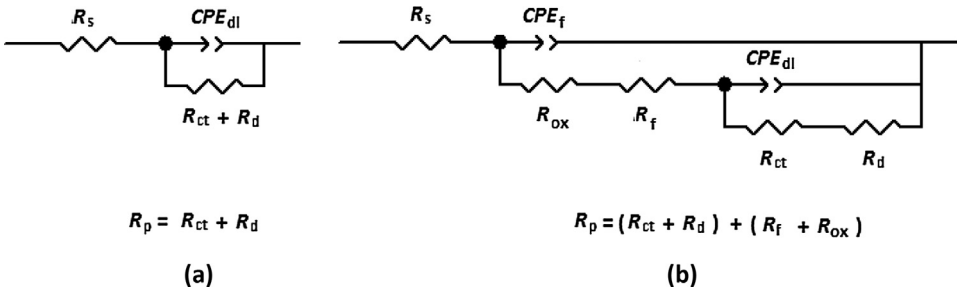

Figure 6 Proposed equivalent circuits for impedance analysis and interpretation of brass-NaCl solution system. Equivalent circuit for having (a) one semi circle (b) two semicircles in impedance spectra.

solution resistance, R_{ct} is the charge transfer resistance, R_d is the diffuse layer resistance which is related to the transportation resistance of ions from metal surface to solution or vice versa (Erbil, 2012) and CPE_{dl} is the constant phase element of the double layer. The semicircle can be described as an overlapping of the double layer resistance (R_{ct}) and the diffuse layer resistance (R_d) in the brass/solution system which are not possible to distinguish between. Therefore the polarization resistance (R_p) can be calculated by summing these two resistances ($R_p = R_{ct} + R_d$).

The equivalent circuit shown in Fig. 6b was used for fitting electrochemical responses of brass which have two loops in the Nyquist plots. As shown in Fig. 6b two different elements were added into the circuit in order to define the brass/solution interface accurately. These added circuit elements were presented as R_f and R_{ox}. R_f reflects the film resistance of adsorbed inhibitor molecules, R_{ox} is the oxide film resistance that formed on brass surface, CPE_f is the constant phase element of the film layers and CPE_{dl} is the constant phase element of the double layer in the equivalent circuit. The nature of the oxide film that formed on brass was explained by Eqs. (3)–(6) given above.

The second loop that can be observed in the Nyquist diagrams of inhibitor free solutions at 308–328 K was related with the oxide layer on brass formed in 3.5% NaCl solution. In these cases there were no inhibitor molecules in the solution, so the film resistance R_f should not take part in the polarization resistance expression. The total resistance may be stated as $R_p = R_{ct} + R_d + R_{ox}$ and CPE_f was related to the oxide film of brass.

In the case of VBB containing solutions, the Nyquist diagrams were described with the equivalent circuit shown in Fig. 6b. In these diagrams there were two loops which were related to the faradaic process and film formation. The faradaic process was associated with the high frequency part of the impedance diagrams and represented with R_{ct}, R_d and CPE_{dl} elements similar to the model mentioned in Fig. 6a. The second loop which was observed in the lower frequency region was attributed to resistance of both the oxide film of brass and the adsorption of VBB. The structure of the protective layer formed on brass in VBB containing solution consisted of both Cu_2O oxide layer and Cu–VBB complex products. We assume that $CuCl_2^-$ species went through the following reactions and Cu(I)VBB complex was formed in the oxide layer. Similar examples are mentioned in literature (Kosec et al., 2008; Quan et al., 2002):

$$x\mathrm{CuCl}_2^- + x\mathrm{VBB} \rightarrow [\mathrm{Cu(I)VBB}]_x + 2x\mathrm{Cl}^- \quad (12)$$

The total polarization resistance can be summed up as $R_p = R_{ct} + R_d + R_{ox} + R_f$ and CPF_f was the capacitance of both oxide and complex film layer.

The data obtained by fitting the EIS results were summarized in Table 2. The R_p values increased significantly with the concentration of VBB whereas the CPE_f values decreased. This suggests that the surface film formed in the presence of VBB was thicker, less permeable and strongly adsorbed (Raj and Rajendran, 2011). The stability of the film did not disappear at high temperatures which is an indication of a strong and stable interaction between the metal and VBB. The inhibition efficiencies were calculated at different concentrations and temperatures utilizing the polarization resistance values according to the following equation.

$$IE\% = \frac{R_{p(\mathrm{Inh})} - R_p}{R_{p(\mathrm{Inh})}} \times 100 \quad (13)$$

where $R_{p(Inh)}$ and R_p are polarization resistance values with and without VBB, respectively.

It is also apparent from Table 2 that the values of CPE_{dl} decreased with increasing VBB concentration. The decrease in CPE_{dl} values suggested a decrease in the dielectric constant and/or an increase in the double layer thickness. This can be explained as a result of adsorption of VBB molecules onto the brass surface which have lesser dielectric constant compared with desorbed water molecules. Thus the brass surface was protected against the corrosive medium (Moretti et al., 2013; Umoren et al., 2014).

The EIS results prove that the inhibition efficiency of VBB increases with increasing concentration of VBB and rising temperature. It was suggested that a stable and strong protective film was formed on the brass surface even at high temperatures.

3.3. Evaluation of SEM and ATR-FTIR results

The brass specimens were exposed to 3.5% NaCl solution for 120 h in the absence and presence of 1.25 mmol/L VBB in order to determine the effect of the immersion time. The measurements were followed by electrochemical impedance method in 24-h interval, and the results were presented as Nyquist and Bode plots in Fig. 7. A representative impedance parameters were given in Table 3 for the corrosion of brass at 24 and 120 h immersion times. The parameters were evaluated using model described in Fig. 6b.

In the beginning of the waiting period of inhibitor free solution, the diameter of capacitive loop increased until the 48th

Table 2 Impedance parameters for the corrosion of brass in 3.5% NaCl at different concentration of VBB and temperatures.

T (K)	C (mmol/L)	R_s (ohm)	CPE_{dl}		$(R_{ct}+R_d)$ (ohm)	CPE_f		$(R_f + R_{ox})$ (ohm)	Rp (ohm)	$IE\%$	θ	χ^2
			Y_0 ($\times 10^6$ s^n ohm^{-1})	n		Y_0 ($\times 10^6$ s^n ohm^{-1})	n					
298	Blank	7.29	68.8	0.80	3910	–	–	–	3910	–	–	0.0010
	0.1	8.19	19.2	0.87	28	53.2	0.56	11,515	11,543	66.1	0.661	0.0052
	0.5	2.91	148.7	0.60	2342	128.5	0.77	10,300	12,642	69.1	0.691	0.0056
	1.0	4.63	25.1	0.67	248	37.7	0.67	21,786	22,034	82.3	0.823	0.0042
	1.25	3.10	11.2	0.73	261	65.6	0.69	35,011	35,272	88.9	0.889	0.0053
308	Blank	4.50	15.0	0.87	23	378.6	0.41	2564	2587	–	–	0.0052
	0.1	5.58	34.5	0.77	5	35.4	0.66	7930	7935	67.4	0.674	0.0037
	0.5	8.39	19.8	0.70	10	36.4	0.76	10,990	10,999	76.5	0.765	0.0010
	1.0	2.62	10.4	0.73	121	84.7	0.62	16,482	16,603	84.4	0.844	0.0021
	1.25	6.24	2.28	0.85	565	25.4	0.58	351	25,503	89.9	0.899	0.0064
318	Blank	5.42	123.8	0.76	1215	8193	0.97	351	1566	–	–	0.0017
	0.1	4.42	49.2	0.75	89	26.8	0.43	5384	5473	71.4	0.714	0.0017
	0.5	1.50	7.4	0.79	369	35.1	0.68	8829	9198	83.0	0.830	0.0087
	1.0	3.16	23.2	0.66	37	12.0	0.47	15,209	15,246	89.7	0.897	0.0348
	1.25	9.96	7.4	0.79	120	28.9	0.56	14,885	15,005	89.6	0.896	0.0329
328	Blank	6.08	694.6	0.58	58	445.3	0.76	672	730	–	–	0.0054
	0.1	4.16	371.1	0.64	478	6864.0	0.68	512	990	26.3	0.403	0.0044
	0.5	3.18	251.0	0.48	59	551.0	0.70	4254	4313	83.1	0.831	0.0035
	1.0	1.00	2.6	0.79	426	79.2	0.61	9766	10,192	92.8	0.928	0.0027
	1.25	2.06	3.8	0.81	272	63.8	0.63	13,836	14,108	94.8	0.948	0.0034

hour (Fig. 7a). This was attributed to the formation of oxide film on brass as mentioned in Eqs. (3)–(6). However, brass was not completely resistant to corrosion in chloride containing media. 48 h later the polarization resistance of brass decreased due to diffusion of chloride ions into oxide layer. This accelerated the dissolution of oxide and the substrate metal lying under the oxide film. The substrate metal also included Zn which is thermodynamically more reactive than copper. Hence Cl^- ions reached to the base metal by opening pores in the oxide film and caused the formation of soluble complex products of metallic zinc as follows (Fan et al., 2011; Ma et al., 2002):

$$Zn + 4Cl^- \rightarrow ZnCl_4^{2-} + 2e^- \quad (14)$$

Meanwhile copper (I) ion could also give soluble products in NaCl environment as have been mentioned above in Eqs. (7)–(9). The cathodic reaction is oxygen reduction like as given in Eq. (2). As can be seen from the Table 3 the polarization resistance of brass in 3.5% NaCl reduced to 6141 from 11,688 ohm 120 h later.

In the case of the solution including 1.25 mmol/L VBB (Fig. 7b), the capacitive loop rapidly increased in diameter to 46,841 ohm within 24 h. A protective film formation caused by the adsorption of VBB molecules on brass surface was suggested. As can be seen in Fig. 7b at 48 h the polarization resistances of brass decreased and afterward remained on the same level. This can be explained as follows: the adsorbed VBB molecules cause an improvement by incorporating into the oxide layer. Mass transfer reaction is controlled this way. The polarization resistance of brass decreased to 22,633 ohm after the exposing time of 120 h. The decrease in the polarization resistance value was caused by the diffusion of corrosive species such as dissolved oxygen and chloride ions into pores of the oxide layer and the electrochemical reactions that was made possible (Solmaz et al., 2008). After 120 h the inhibition efficiency of VBB seemed to be 72.9% which suggested that the inhibitor film was reasonably permanent.

The SEM images of brass surfaces exposed to 3.5% NaCl without and with 1.25 mmol/L VBB for 120 h are given on Figs. 8 and 9.

SEM examination of the figures clearly shows the difference between the two brass surfaces. The damage that the metal suffered in the absence of VBB is clearly seen in Fig. 8a and b. Small sized corrosion products and pits that spread over the surface of brass were observed in inhibitor free NaCl solution.

Fig. 9a and b shows the brass surface that was exposed to 3.5% NaCl + 1.25 mmol/L VBB solution for 120 h. The polishing scratches on the brass surface could be seen even 120 h later from the figures. There were no corrosion products and cracks on brass surface in the VBB containing solution which proves that the metal was hindered against corrosive species. When comparing the surface treated with 3.5% NaCl + 1.25 mmol/L VBB solution to the surface treated with 3.5% NaCl solution a smoother surface was observed.

After exposing the substrate for 120 h in NaCl + 1.25 mmol/L VBB solution, ATR-FTIR of brass surface was recorded in order to confirm the adsorption of the VBB film on the metal surface. ATR-FTIR spectrum of untreated brass surface was also recorded to make comparison with the inhibited brass surface and it was shown in Fig. 10. As can be seen from the figure the characteristic band of N–H stretching is indicated by peak at 3389 cm^{-1}, peak at 1431 cm^{-1} corresponding to C–C stretching and the peak at 1243 cm^{-1} corresponding to C–N stretching (Radoi et al., 2008). These observations prove the existence of VBB on the brass surface after exposing 120 h to corrosive medium.

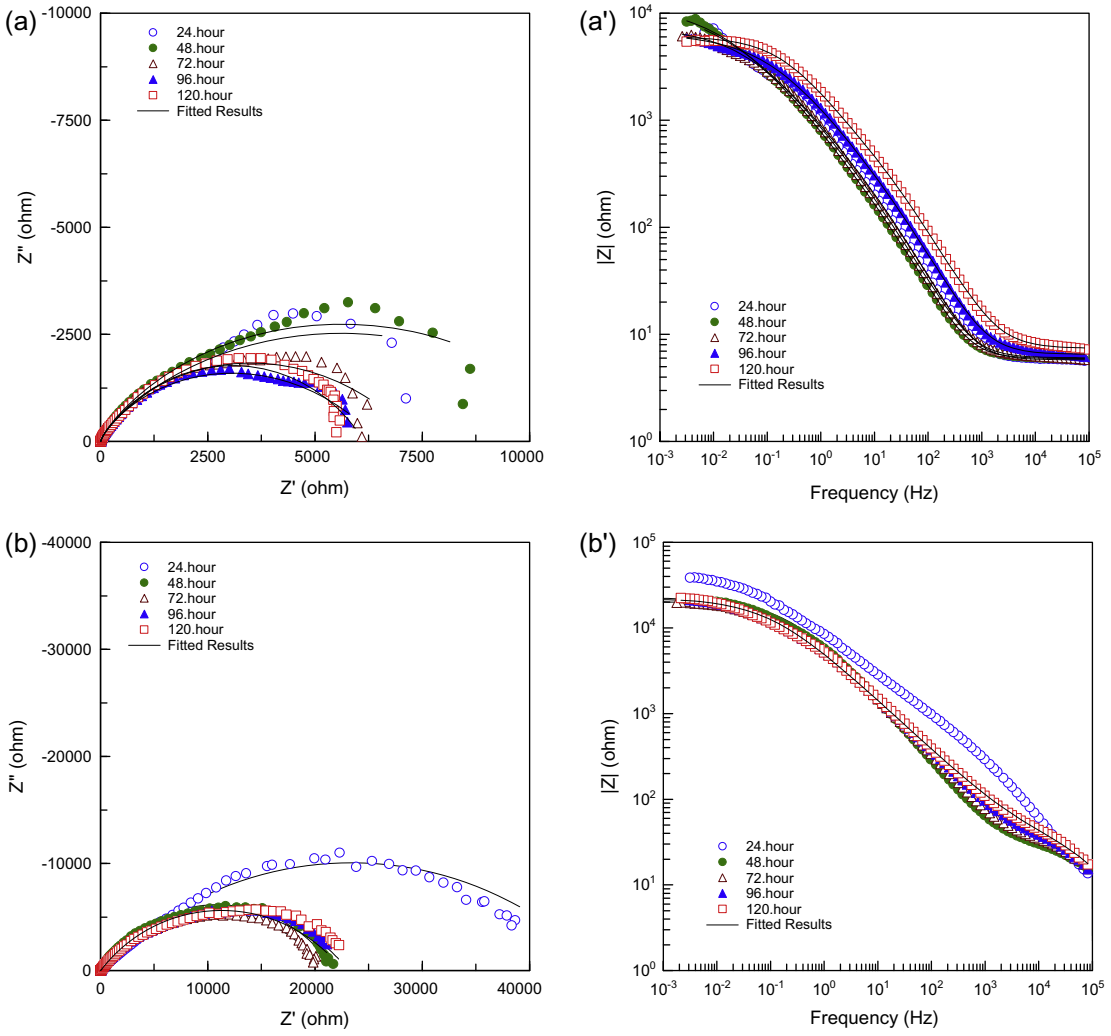

Figure 7 Nyquist and Bode plots of brass in 3.5% NaCl solution absence (**a** and **a′**) and (**b** and **b′**) presence of 1.25 mmol/L VBB at different immersion times: 24 h (○), 48 h (●), 72 h (△), 96 h (▲) and 120 h (□).

Table 3 Impedance parameters for the corrosion of brass in 3.5% NaCl solution and 3.5% NaCl + 1.25 mmol/L VBB solution at different immersion times.

	Immersion time (h)	R_s (ohm)	CPE_{dl}		$(R_{ct}+R_d)$ (ohm)	CPE_f		$(R_f + R_{ox})$ (ohm)	Rp (ohm)	$IE\%$	χ^2
			Y_0 ($\times 10^6$ s^n ohm^{-1})	n		Y_0 ($\times 10^6$ s^n ohm^{-1})	n				
3.5% NaCl	24	5.78	81.8	0.91	147	321	0.49	11,541	11,688	–	0.0094
	120	7.40	49.7	0.84	722	121	0.61	5419	6141	–	0.0044
3.5%NaCl + VBB	24	4.05	2.9	0.78	689	39.3	0.51	46,152	46,841	75.0	0.0009
	120	5.87	0.1	0.98	20	59.4	0.59	22,613	22,633	72.9	0.0036

3.4. Adsorption isotherms

The adsorption isotherm describes the interaction of inhibitor molecules with the metal surface which is important when evaluating the mechanism of the inhibition. If an organic molecule adsorbed on metal efficiently, it can be called a successful corrosion inhibitor. The adsorption process occurs between the metal/solution interface by replacing adsorbed water molecules and organic molecules as shown in the reaction given below (15) (Mistry et al., 2013).

$$Org_{(sol)} + mH_2O_{(ads)} \leftrightarrow Org_{(ads)} + mH_2O_{(sol)} \quad (15)$$

In this equilibrium reaction, the organic molecules in the solution and adsorbed molecules on the metal surface are represented as $Org_{(sol)}$ and $Org_{(ads)}$, respectively, and m is the number of water molecules that is replaced with organic

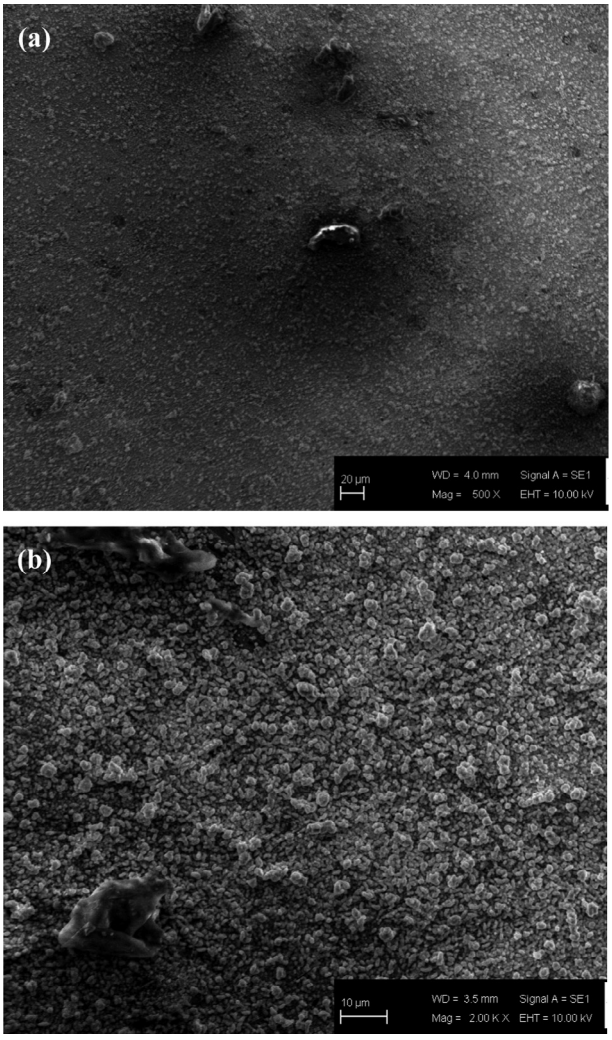

Figure 8 SEM images of brass surface exposed to 3.5% NaCl solution for 120 h at 298 K. (a) Magnification ×500 and (b) Magnification ×2000.

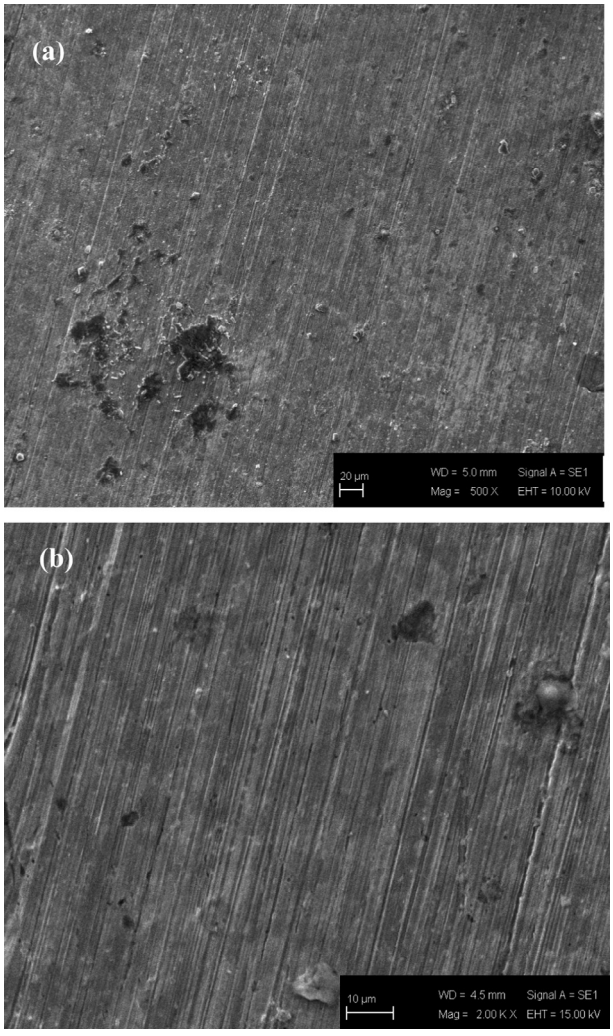

Figure 9 SEM images of brass surface exposed to 3.5% NaCl + 1.25 mmol/L VBB solution for 120 h at 298 K. (a) Magnification ×500 and (b) Magnification ×2000.

molecules. To determine which adsorption isotherm best fits the adsorption mode of VBB on brass, the surface coverage (θ) values were used in different isotherms. The plots were obtained by using inhibition efficiencies that were calculated from potentiodynamic polarization measurements. The values seemed to fit best with the Langmuir adsorption isotherm with correlation coefficients which have been given in Fig. 11. The Langmuir adsorption isotherm can be expressed as in Eq. (16).

$$\frac{C_{\text{inh}}}{\theta} = \frac{1}{K_{\text{ads}}} + C_{\text{inh}} \tag{16}$$

In the equation, θ shows the degree of coverage on the metal surface, C_{inh} represents the inhibitor concentration and K_{ads} represents the equilibrium constant of adsorption process.

High correlation coefficients approved the consistency of experimental results with the Langmuir adsorption isotherm. Therefore, it was concluded that the adsorbed molecules aligned on the metal surface without interactions between adjacent molecules (Obot et al., 2009).

K_{ads}, the equilibrium constant of the adsorption process, was calculated from the reciprocal of the intercept of the plotted isotherm line (Fig. 11). Subsequently, K_{ads} was used to evaluate the standard free energy of adsorption ($\Delta G^{\text{o}}_{\text{ads}}$) values of the VBB molecule at each temperature by the following Eq. (17):

$$K_{\text{ads}} = \frac{1}{C_{\text{Solvent}}} \exp \frac{-\Delta G^{\text{o}}_{\text{ads}}}{\text{RT}} \tag{17}$$

where C_{solvent} is the molar concentration of water which is 55.5 mol L^{-1}, R is the gas constant (8.314 J K^{-1} mol^{-1}) and T is the absolute temperature (K).

The calculated values of K_{ads} and $\Delta G^{\text{o}}_{\text{ads}}$ were listed in Table 4. The $\Delta G^{\text{o}}_{\text{ads}}$ values were −37.0; −36.8; −37.9 and −39.9 kJ mol^{-1} respectively at the temperature range of 298–328 K. The negative values of $\Delta G^{\text{o}}_{\text{ads}}$ mean that the adsorption process of VBB on brass surface is spontaneous. Generally, $\Delta G^{\text{o}}_{\text{ads}}$ values around −20 kJ mol^{-1} are accepted as a physisorption which takes place by an electrostatic interaction between charged molecules and the metal; those around −40 kJ mol^{-1} are known as chemisorption. Chemisorption requires charge sharing or transfer between an organic molecule and metal which causes them to co-ordinate and form a

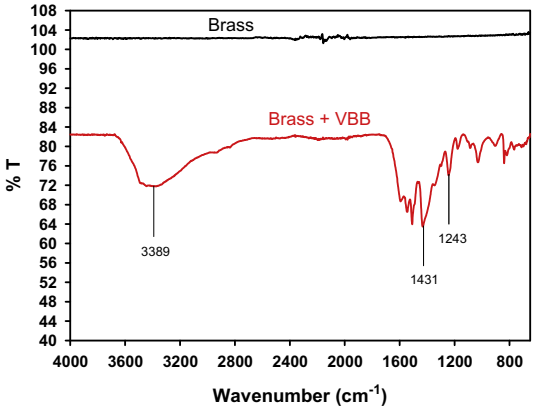

Figure 10 Ex-situ ATR-FTIR spectra of brass surface recorded after exposing 120 h in 3.5% NaCl solution with and without VBB in the wave number region 4000–650 cm^{-1}.

covalent bond (Liao et al., 2011). The fact that the ΔG^{o}_{ads} values are very close to -40 kJ mol^{-1} indicates that the adsorption of VBB is not merely a physical or a chemical adsorption. Therefore, the adsorption of VBB on brass surface can be accepted as a mixed type of adsorption which has a chemical contribution on a physical adsorption. Similar results are reported in literature (Ramesh and Adhikari, 2009; Ali et al., 2005; Noor and Al-Moubaraki, 2008).

3.5. Activation energy calculations

Temperature investigations are important in corrosion studies because they make it possible to determine the activation energy (E_a) and calculate the dissolution process. Information about the inhibition mechanism can be collected by comparing E_a values both in the presence and absence of the inhibitor (Popova et al., 2007). Therefore, the corrosion rate of brass in 3.5% NaCl solution alone and with the presence of VBB was determined at different temperatures for E_a calculation.

Table 4 Adsorption equilibrium constants (K_{ads}) and standard free energy of adsorption (ΔG^{o}_{ads}) of VBB on brass in 3.5% NaCl solution.

Temperature (K)	K_{ads} ($\times 10^4$ L/mol)	ΔG^{o}_{ads} (kJ mol^{-1})
298	5.56	−37.0
308	3.13	−36.8
318	3.03	−37.9
328	4.05	−39.9

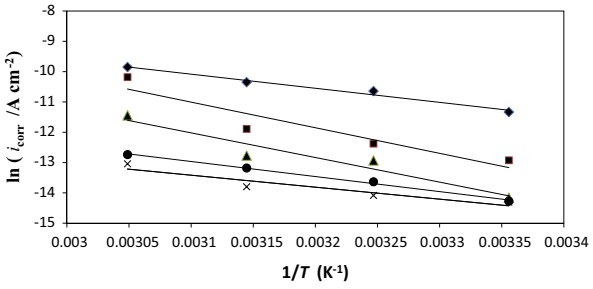

Figure 12 Arrhenius plots of brass corrosion in 3.5% NaCl solution in presence of (♦) 3.5% NaCl; (■) 0.1 mmol/L VBB; (▲) 0.5 mmol/L VBB; (●)1.0 mmol/L VBB; and (×) 1.25 mmol/L VBB.

The relation between corrosion rate and temperature is given in the Arrhenius Eq. (18) (Bahrami et al., 2010):

$$i_{corr} = A \exp(-E_a/RT) \quad (18)$$

Here A is a constant, i_{corr} is corrosion current density, E_a is the activation energy, R is the universal gas constant and T is the absolute temperature. Fig. 12 represents the Arrhenius plots of the [ln i_{corr} vs. $1/T$] for brass in 3.5% NaCl solution. From the slopes of these plots E_a values were calculated and given in Table 5.

The E_a values were 38.65 kJ mol^{-1}; 70.21 kJ mol^{-1}; 67.53 kJ mol^{-1}; 41.24 kJ mol^{-1}; 32.85 kJ mol^{-1} for the absence and presence of VBB with increasing concentrations,

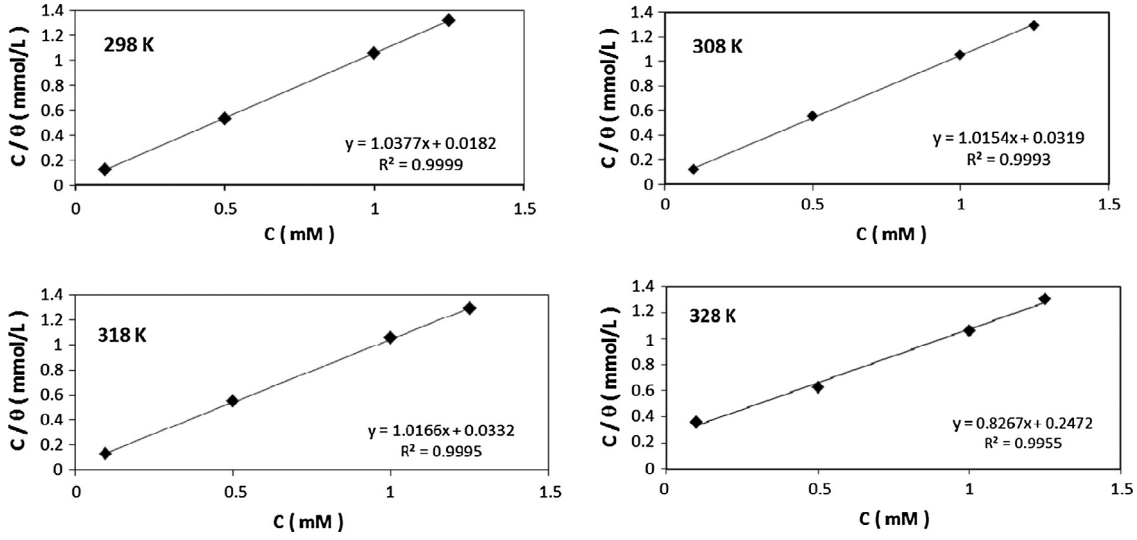

Figure 11 Langmuir adsorption plots of VBB on brass in 3.5% NaCl solution at 298–328 K temperatures.

Table 5 Activation energy values, E_a, for the corrosion of brass in 3.5% NaCl solution with and without different concentration of VBB and temperature dependence of percent inhibition efficiency, *IE*%. (E_a = kJ mol^{-1}).

T (K)	3.5% NaCl		0.1 mmol/L VBB		0.5 mmol/L VBB		1.0 mmol/L VBB		1.25 mmol/L VBB	
	E_a	*IE*%	E_a	*IE*%	E_a	IE%	E_a	*IE*%	E_a	*IE*%
298	38.65	–	70.21	79.6	67.53	94.1	41.24	94.7	32.85	94.9
308		–		82.3		89.9		95.0		96.8
318		–		78.6		91.1		94.1		96.8
328		–		28.2		79.7		94.4		95.9

respectively. The E_a values obtained in the presence of VBB were found higher (except 1.25 mmol/L VBB) when compared to the values obtained in the absence of VBB. The lowest E_a was observed in solution including 1.25 mmol/L M of VBB. According to some researchers (Keleş, 2011; Kardaş, 2005; Bouklah et al., 2006) the increase in E_a value in the presence of the inhibitor refers to the physical adsorption and the opposite case has been attributed to the chemisorption. In our study the adsorption of VBB seems to be physical except at the highest VBB concentration. Similar behavior was reported by Ali et al.(2005) who deduced that change of adsorption type is connected with increasing inhibitor concentration. This situation was related with the decrease of the frequency factor and change in the dissolution mechanism. Hence the adsorption was referred to as chemisorption with higher concentration range and physisorption with lower concentration range. Oguzie et al. (2005) have reported that because some energy is used in chemisorption, a decrease in activation energy is observed in the corrosion process of inhibitor containing systems compared with blank solution. Physisorption may have taken place in metal/solution interface when an increase is observed in the activation energy of the inhibited systems.

The temperature dependence of percent inhibition efficiency (*IE*%) is also shown in Table 5. The metal surface was covered with inhibitor molecules even at higher temperatures, and rate determining step of the metal dissolution becomes diffusion controlled through the film of corrosion products and inhibitor. The rate of metal dissolution can be considered as a sum of corrosion rate of the bare metal and corrosion rate on this part of the surface which is covered by adsorbed inhibitor. At high degrees of coverage, the first process has no substantial contribution (Behpour et al., 2010). In this case the corrosive mechanism includes a direct reaction of the molecules of the inhibitor with the metal surface and the activation energy can be smaller or higher than in absence of inhibitor. According to these; the higher value of E_a in uninhibited solution compared with inhibited solution and increase of its *IE*% with temperature increase can be interpreted as an indication of transformation of physical adsorption into chemical adsorption.

Taking the references and the results obtained from the activation energy calculations into consideration, it can be concluded that the adsorption of VBB could not be classified as simply physical or chemical. Previous standard free energy finding supports this suggestion. We can say that a strong physisorption process may take place at lower concentrations and chemical interactions may contribute to the adsorption of VBB at the highest concentrations.

4. Conclusions

According to experimental findings we can present the following remarks.

VBB exhibited very good corrosion inhibition performance for brass in 3.5% (w/v) NaCl solution at the temperature range of 298–328 K. Potentiodynamic polarization and EIS results reveal that VBB inhibits the corrosion of brass in aggressive NaCl solution even at 328 K temperature with 95.9% and 95.1%. VBB acts as a mixed type inhibitor at all studied temperatures and it reduces both anodic and cathodic reactions. The adsorption of VBB on brass surface in 3.5% NaCl solution was found to follow the Langmuir adsorption isotherm. Standard free energy of adsorption (ΔG^{o}_{ads}) values suggested that VBB is tightly adsorbed on the brass surface. It can be said that physisorption process takes place at lower concentrations of VBB and chemical interactions contribute to the adsorption in the higher concentration range. ATR-FTIR spectroscopy techniques were used to prove the existence of the VBB inhibitor film. SEM results showed a smoother surface in the VBB containing solutions when was compared with the inhibitor free solution. This suggested that the metal has been hindered against corrosive species 120 h later.

Acknowledgement

Osmaniye Korkut Ata University is gratefully acknowledged for instrumental support. The authors would also like to thank Murat Farsak¸ for his valuable help during ATR-FTIR measurements.

References

Ahamad, I., Prasad, R., Quraishi, M.A., 2010. Thermodynamic, electrochemical and quantum chemical investigation of some Schiff bases as corrosion inhibitors for mild steel in hydrochloric acid solutions. Corros. Sci. 52, 933–942.

Ali, S.A., El-Shareef, A.M., Al-Ghamdi, R.F., Saeed, M.T., 2005. The isoxazolidines: the effects of steric factor and hydrophobic chain length on the corrosion inhibition of mild steel in acidic medium. Corros. Sci. 47, 2659–2678.

Antonijevic, M.M., Milic, S.M., Serbula, S.M., Bogdanovic, G.D., 2005. The influence of chloride ions and benzotriazole on the corrosion behavior of Cu37Zn brass in alkaline medium. Electrochim. Acta 50, 3693–3701.

Antonijevic, M.M., Milic, S.M., Radovanovic, M.B., Petrovic, M.B., Stamenkovic, A.T., 2009. Influence of pH and chlorides on electrochemical behavior of brass in presence of benzotriazole. Int. J. Electrochem. Sci. 4, 1719–1734.

Bahrami, M.J., Hosseini, S.M.A., Pilvar, P., 2010. Experimental and theoretical investigation of organic compounds as inhibitors for mild steel corrosion in sulfuric acid medium. Corros. Sci. 52, 2793–2803.

Behpour, M., Ghoreishi, S.M., Mohammadi, N., Soltani, N., Slavati-Niasari, M., 2010. Investigation of some Schiff base compounds containing disulfide bond as HCl corrosion inhibitors for mild steel. Corros. Sci. 52, 4046–4057.

Bouklah, M., Hammouti, B., Lagrenee, M., Bentiss, F., 2006. Thermodynamic properties of 2,5-bis(4-methoxyphenyl)-1,3,4-oxadiazole as a corrosion inhibitor for mild steel in normal sulfuric acid medium. Corros. Sci. 48, 2831–2842.

Erbil, M., 2012. Korozyon: İlkeler ve Önlemler. The Corrosion Association Publication, Ankara, Turkey.

Fan, H., Li, S., Zhao, Z., Wang, H., Shi, Z., Zhang, L., 2011. Inhibition of brass corrosion in sodium chloride solutions by self-assembled silane films. Corros. Sci. 53, 4273–4281.

Fengling, X., Jizhou, D., Shufang, Z., Baorong, H., 2008. The inhibition of mild steel corrosion in 1 M hydrochloric acid solutions by triazole derivative. Mater. Lett. 62, 4072–4074.

Gao, G., Liang, C.H., 2007. 1,3-Bis-diethylamino-propan-2-ol as volatile corrosion inhibitor for brass. Corros. Sci. 49, 3479–3493.

Gerengi, H., Bereket, H., 2012. Adsorption and inhibition effect of Benzotriazole on Brass-118 and Brass-MM55in artificial seawater. Prot. Met. Phys. Chem. Surf. 48, 361–366.

Gerengi, H., Darowicki, K., Bereket, G., Slepski, P., 2009. Evaluation of corrosion inhibition of brass-118 in artificial seawater bybenzotriazole using Dynamic EIS. Corros. Sci. 51, 2573–2579.

Gerengi, H., Darowicki, K., Slepski, P., Bereket, G., Ryl, J., 2010. Investigation effect of benzotriazole on the corrosion of brass-MM55 alloy in artificial seawater by dynamic EIS. J. Solid State Electr. 14, 897–902.

Kardaş, G., 2005. The inhibition effect of 2-thiobarbituric acid on the corrosion performance of mild steel in HCl solutions. Mater. Sci. 41, 337–343.

Kear, G., Barker, B.D., Stokes, K.R., Walsh, F.C., 2005. Corrosion and impressed current cathodic protection of copper-based materials using a bimetallic rotating cylinder electrode (BRCE). Corros. Sci. 47, 1694–1705.

Keleş, H., 2011. Electrochemical and thermodynamic studies to evaluate inhibition effect of 2-[(4-phenoxy-phenylimino)methyl]-phenol in 1M HCl on mild steel. Mater. Chem. Phys. 130, 1317–1324.

Kosec, T., Milosev, I., Pihlar, B., 2007. Benzotriazole as an inhibitor of brass corrosion in chloride solution. Appl. Surf. Sci. 253, 8863–8887.

Kosec, T., Merl, D.K., Milosev, I., 2008. Impedance and XPS study of benzotriazole films formed on copper, copper-zinc alloys and zinc in chloride solution. Corros. Sci. 50, 1987–1997.

Liao, Q.Q., Yue, Z.W., Yang, D., Wang, Z.H., Li, Z.H., Ge, H.H., Li, Y.J., 2011. Inhibition of copper corrosion in sodium chloride solution by the self-assembled monolayer of sodium diethyldithiocarbamate. Corros. Sci. 53, 1999–2005.

Ma, H., Chen, S., Niu, L., Zhao, S., Li, S., Li, D., 2002. Inhibition of copper corrosion by several Schiff bases in aerated halide solutions. J. Appl. Electrochem. 32, 65–72.

Mistry, B.M., Sahoo, S.K., Jauhari, S., 2013. Experimental and theoretical investigation of 2-mercaptoquinoline-3-carbaldehyde and its Schiff base as an inhibitor of mild steel in 1 M HCl. J. Electroanal. Chem. 704, 118–129.

Moretti, G., Guidi, F., Fabris, F., 2013. Corrosion inhibition of the mild steel in 0.5 M HCl by 2-butyl-hexahydropyrrolo[1,2-b][1,2]oxazole. Corros. Sci. 76, 206–218.

Mountassir, Z., Srhiri, A., 2007. Electrochemical behaviour of Cu–40Zn in 3% NaCl solution polluted by sulphides: effect of aminotriazole. Corros. Sci. 49, 1350–1361.

Negm, N.A., Zaki, M.F., Said, M.M., Morsy, S.M., 2011. Inhibitory action of biodegradable modified vanillin on the corrosion of carbon steel in 1 M HCl. Corros. Sci. 53, 4233–4240.

Noor, E.A., Al-Moubaraki, A.H., 2008. Thermodynamic study of metal corrosion and inhibitor adsorption processes in mild steel/1-methyl-4[4′(-X)-styryl pyridinium iodides/hydrochloric acid systems. Mater. Chem. Phys. 110, 145–154.

Obot, I.B., Obi-Egbedi, N.O., Umoren, S.A., 2009. Antifungal drugs as corrosion inhibitors for aluminium in 0.1 M HCl. Corros. Sci. 51, 1868–1875.

Oguzie, E.E., Onuoha, G.N., Onuchukwu, A.I., 2005. Inhibitory mechanism of mild steel corrosion in 2 M sulphuric acid solution by methylene blue dye. Mater. Chem. Phys. 89, 305–311.

Oguzie, E.E., Li, Y., Wang, F.H., 2007. Corrosion inhibition and adsorption behavior of methionine on mild steel in sulfuric acid and synergistic effect of iodide ion. J. Colloid Interf. Sci. 310, 90–98.

Özcan, M., 2008. AC impedance measurement of cystine adsorption at mild steel/sulfuric acid interface as corrosion inhibitör. J. Solid State Electr. 12, 1653–1661.

Özkir, D., Bayol, E., Gürten, A.A., Sürme, Y., Kandemirli, F., 2013. Effect of hyamine on electrochemical behaviour of brass alloy in HNO_3 solution. Chem. Pap. 67, 202–212.

Popova, A., Christov, M., Vasilev, A., 2007. Inhibitive properties of quaternary ammonium bromides of N-containing heterocycles on acid mild steel corrosion. Part I: Gravimetric and voltammetric results. Corros. Sci. 49, 3276–3289.

Qi, K., Qiu, Y., Chen, Z., Guo, X., 2013. Corrosion of conductive polypyrrole: effects of continuous cathodic and anodic polarization. Corros. Sci. 69, 376–388.

Quan, Z., Chen, S., Li, Y., Cui, X., 2002. Adsorption behaviour of Schiff base and corrosion protection of resulting films to copper substrate. Corros. Sci. 44, 703–715.

Radoi, A., Compagnone, D., Valcarcel, M.A., Placidi, P., Materazzi, S., Moscone, D., Palleschi, G., 2008. Detection of NADH via electrocatalytic oxidation at single-walled carbon nanotubes modified with Variamine blue. Electrochim. Acta 53, 2161–2169.

Raj, X.J., Rajendran, N., 2011. Corrosion inhibition effect of substituted Thiadiazoles on Brass. Int. J. Electrochem. Sci. 6, 348–366.

Ramesh, S.V., Adhikari, A.V., 2009. N′-[4-(Diethylamino) benzylidine]-3-{[8-(trifluoromethyl) quinolin-4-yl]thio}propano hydrazide) as an effective inhibitor of mild steel corrosion in acid media. Mater. Chem. Phys. 115, 618–627.

Ravichandran, R., Rajendran, N., 2005. Electrochemical behaviour of brass in artificial seawater: effect of organic inhibitors. Appl. Surf. Sci. 239, 449–458.

Ravichandran, R., Nanjundan, S., Rajendran, N., 2004. Effect of benzotriazole derivatives on the corrosion of brass in NaCl solutions. Appl. Surf. Sci. 236, 241–250.

Solmaz, R., Kardaş, G., Yazıcı, B., Erbil, M., 2008. Adsorption and corrosion inhibitive properties of 2-amino-5-mercapto-1,3,4-thiadiazole on mild steel in hydrochloric acid media. Colloid. Surf. A 312, 7–17.

Solmaz, R., Şahin, E.A., Döner, A., Kardaş, G., 2011. The investigation of synergistic inhibition effect of rhodanine and iodide ion on the corrosion of copper in sulphuric acid solution. Corros. Sci. 53, 3231–3240.

Umoren, S.A., Solomon, M.M., Eduok, U.M., Obot, I.B., Israel, A.U., 2014. Inhibition of mild steel corrosion in H_2SO_4 solution by coconut coir dust extract obtained from different solvent systems and synergistic effect of iodide ions: Ethanol and acetone extracts. J. Environ. Chem. Eng. 2, 1048–1060.

Xavier, J.R., Nanjundan, S., Rajendran, N., 2012. Electrochemical adsorption properties and inhibition of brass corrosion in natural seawater by thiadiazole derivatives: experimental and theoretical investigation. Ind. Eng. Chem. Res. 51, 30–42.